Available online at www.sciencedirect.com

Manufacturing Letters

Manufacturing Letters 41 (2024) 536–545

52nd SME North American Manufacturing Research Conference (NAMRC 52, 2024)

Surface integrity analysis and inspection for nanochannel sidewalls using the self-affine fractal model-based statistical quality control for the atomic force microscopy (AFM)-based nanomachining process

Xinchen Wang, Mohammad Alshoul, Jia Deng, Zimo Wang*

Department of Systems Science and Industrial Engineering, Binghamton University, Binghamton, NY 13902, USA
* Corresponding author. Tel.:+1-607-777-5012. *.E-mail address:* zimowang@binghamton.edu

Abstract

The atomic force microscopy (AFM) technology is a promising method for nanofabrication due to the high tunability of this affordable platform. The quality inspection and control significantly impact the manufacturing effectiveness for realizing the functionality of the achieved nanochannel. Particularly, the surface characteristics of nanochannel sidewalls, which play a significant role in determining the quality of the nanomachined products, can not be accurately captured using conventional surface integrity metrics (e.g., surface roughness). Therefore, it is necessary to propose a method to quantitatively characterize the surface morphology and detect the abnormal parts/regions of the nanochannel sidewall. This paper presents a statistical process control approach derived from the self-affine fractal model to detect the sidewall surface anomalies. It evaluates changes in the self-affine fractal model parameters (standard deviation, correlation length, and roughness exponent), which can be used to signify the changes on the sidewall surface; the statistical distributions of these parameters are derived and used to develop control charts to allow inspection of the sidewall morphology. The approach was tested on the AFM-based nanomachined samples. The results suggest that the presented approach can effectively reflect the abnormal regions on the machined parts, which opens up a new avenue toward guiding the quality control and rework for process improvement for AFM-based nanomachining.

Peer-review under responsibility of the scientific committee of the NAMRI/SME.
Keywords: Atomic force microscopy; Nanofabrication; Sidewall roughness; Self-affine fractal model; Quality control

1. Introduction

The atomic force microscopy (AFM)-based nanofabrication technology can realize functional surfaces under the nanoscale. It has gleaned attention from various industries due to its low cost [1], simple operation [2], and high accuracy advantages [3] [4]. Due to the difficulty and time-consuming procedures of the AFM-based scanning process, quantitively characterizing surface characteristics for AFM is low efficient. Therefore, quality inspection and control are critical to ensure productivity and provide guidance on the rework and process improvements [5] [6].

Accurate measurement of these nanoscale products is important for obtaining the fundamental characteristics of these products and ensuring the corresponding device's performance [7] [8]. Roughness characterization of the nanochannel sidewall plays a significant role in the quality evaluation of the nanofabrication, which can impact the performance of the semiconductor transistors and optical waveguides in Si photonics [9]. The LER (line edge roughness) and LWR (line width roughness) were used to study the performance of the process and characterize the critical dimension (CD) for achieved nanofabricated surface profiles [10]. These two metrics are basic parameters to characterize the surface consistency: the correlation between the LER and LWR was studied to accurately depict the achieved trench morphology [11] [12]. However, conventional quantifiers, such as LER, LWR, bearing area curves, and surface roughness values [R_a (mean roughness), R_q (root mean square), and R_Z (roughness

Peer-review under responsibility of the scientific committee of the NAMRI/SME.

depth)], can only reflect the amplitude changes in first and second orders of statistics, or they are only suitable for 2D profile with limited ability to distinguish between different surface textures [13]. These conventional statistical quantifiers failed to reflect the part-to-part variations for the line edge roughness under the nanoscale [14]. For example, the surface rougness quantifier R_q (root mean squared of the profile) of the sidewall roughness (two profile lines also with comparable R_a values) can only depict the sidewall roughness from the time series, which cannot show the spectral property of the morphology of the sidewall. The following simulated profile lines have the same R_q values, but the morphology differs, indicating that conventional profile quantifiers are insufficient to reflect the roughness of the sidewall, especially on the geometry under the nanoscale.

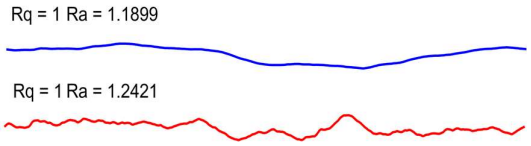

Fig. 1. Two simulated profile lines with similar roughness values

Therefore, to characterize the achieved nanochannel surface characteristics at the nanoscale, advanced approaches need to be applied to represent the changes in functional surface characteristics quantitively. The line edge is based on the different scales and frequencies. This motivates us to present an analytic framework for surface characteristics evaluations for nanofabrication processes.

Researchers have been investigating quantifiers to evaluate the integrity of the functional surface in precision manufacturing. The power spectral density analysis (PSD) is a promising method to analyze the profile variations of achieved surface morphology in the frequency domain [15]. To quantify the texture of the featured surfaces, the PSD was used to analyze the line pattern dataset from an EUV (Extreme ultraviolet lithography) ADI (After development inspection) wafer, which can provide the wafer signature maps of various metrics of interest and achieve the model correlation and process control for the scanner process [16]. To simulate accurate surface topography, the PSD in different dimensions and height probability distribution was analyzed to generate the perfect surface with the desired autocorrelation response [17] [18]. To overcome the noise effects in SEM (Scanning electron microscopy)-based LER metrology, a deep learning method combined with PSD and Poisson denoising method was used to acquire the unbiased LER metrology for line patterns under nanoscale [19] [20]. In addition to the frequency domain informatics, the autocorrelation function and height-height correlation function describe the relationship between the two points on the line edge position, which can be used to estimate the roughness parameters and describe the property of the line edge roughness [21] [22]. However, most existing approaches can only reflect one property for surface profiles. It is insufficient to describe the nanochannel characteristics comprehensively.

In addition, most research only focused on the line edge roughness (LER) analysis on the sample surface rather than the sidewall of the achieved trenches during the nanofabrication. Detection of the sidewall damage is also significant for the nanofabrication evaluation, and the different damage modes indicate various machining processes [23]. Meanwhile, the sidewall roughness is also an essential indicator for evaluating the different nanofabrication technologies that can be used to compare the surface condition of the sidewall before and after the process [24]. Therefore, the quality issue of nanochannels' sidewall impacts the manufacturing effectiveness and the technology selection. To accurately measure the sidewall profiles, the metrological tilting-AFM is used to acquire the line pattern on the vertical sidewall, and LER and PSD were used to analyze the changes of the roughness on the sidewall [25] [26]. In addition, a 3D-AFM with automatic sidewall roughness (SWR) program is proposed to measure the SWR in the semiconductor industry, which can effectively improve the measurement speed and reliability [27]. To ensure the resolution, a new Payne–Lacey Bending model was proposed to measure the sidewall roughness under sub-nanometers using AFM [28].

The self-affine fractal model has been reported to distinguish the roughness profiles with fine texture changes via its three parameters: standard deviation (σ), correlation length (ξ), and roughness exponent (α) [29]. Most related reports used these parameters as significant indicators to distinguish the line edge roughness achieved by various methods and compare the surface morphology before and after treatment [30] [31]. However, very few studies have been reported to adopt such a model to characterize the achieved line edges (or side walls of nanotrenches) and functional surface profile. This is mainly due to the lack of explicit quantification/diagnosis approaches to signify the self-affine fractal model to the changes in the surface characteristics under nanoscale.

In this paper, we investigated the surface characteristics of the AFM-based nanofabrication and presented a quality control process for the obtained trenches according to their sidewall roughness. The LER on different height levels of the trench sidewalls is acquired and analyzed based on the self-affine fractal model. The statistical distribution of the parameters from the self-affine fractal model is studied and used to achieve quality control for the sample morphology under nanoscale.

The remainder of the paper is organized as follows. Sec. 2 presents the setup of the experiments and data acquired from the experimental sample. The method for the surface roughness analysis and quality control of the trench sidewall is introduced in Sec. 3. The results of the quality control analysis for sidewall roughness are discussed in Sec. 4, followed by the concluding remarks in Sec. 5.

2. Experimental setup and data collection

The setup of experiments and related parameters are shown in Fig. 2 [32] [33] [34]. The surface morphology of each trench under various conditions is shown in Fig. 3 (a), and the cross-section profiles of the fabricated sample are shown in Fig. 3 (b). The depth of the trenches ranges from 2nm to 20nm, and the width ranges from 20nm to 90nm.

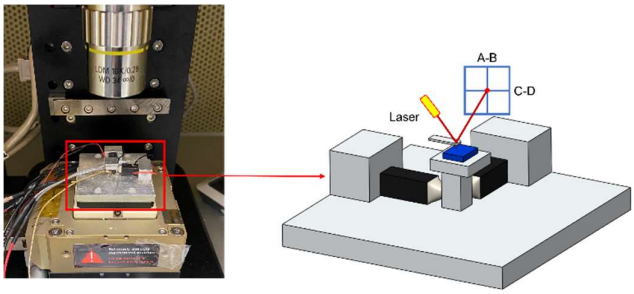

Fig. 2. AFM-based nanofabrication experiment was conducted on a commercial AFM system (Park- XE7 AFM system) with a designed nanovibrator platform; PMMA sample with 200 nm thickness was spin-coated on silicon substrates with post-bake at 180˚C for 90 seconds. DLC190 AFM probe was used to fabricate and image the nanotrenches.

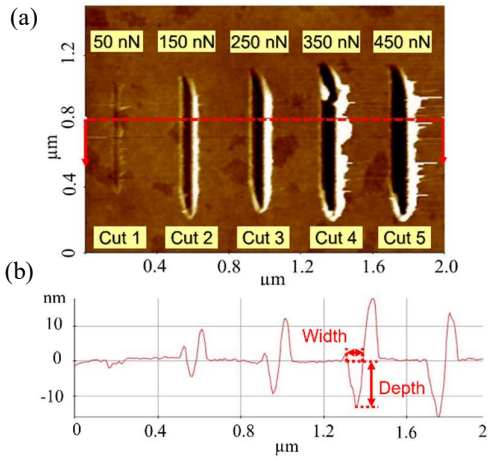

Fig. 3. (a) Five nanomachined trenches; (b) Cross-sectional profile with widths and depths of the trenches.

2.1. Data description

To further investigate the detailed profiles of the trenches and quantify the evaluation process, we used AFM technology to scan the fabricated sample and remap the surface morphology using the contour lines of the sample in Fig. 4 (a). The total sample area is 2×1.5 micrometers, and five cuts from left to right are machined by various forces (50, 150, 250, 350, and 450 nNs). For the roughness analysis of the sidewall, the contour lines of each trench under the 0 z-axis can reflect the roughness characterization of the sidewall. To observe the sidewall surface of the trench, we segmented the obtained model from the middle part of the trench in Fig. 4 (a), and the morphology of the left sidewall of the trench (Cut 3) is shown in Fig. 4 (b) and (c). From Fig. 4, we can observe that the sidewall of the trench is not a smooth surface, with roughness varying from the bottom to the top area. The rough sidewall of the nanotrenches can influence the performance of the cutting trenches under nanoscale, which can not be perfectly noticed by analyzing the edge roughness on the surface. Therefore, the roughness analysis of the trench sidewall is essential for evaluating the quality of the achieved nanotrenches.

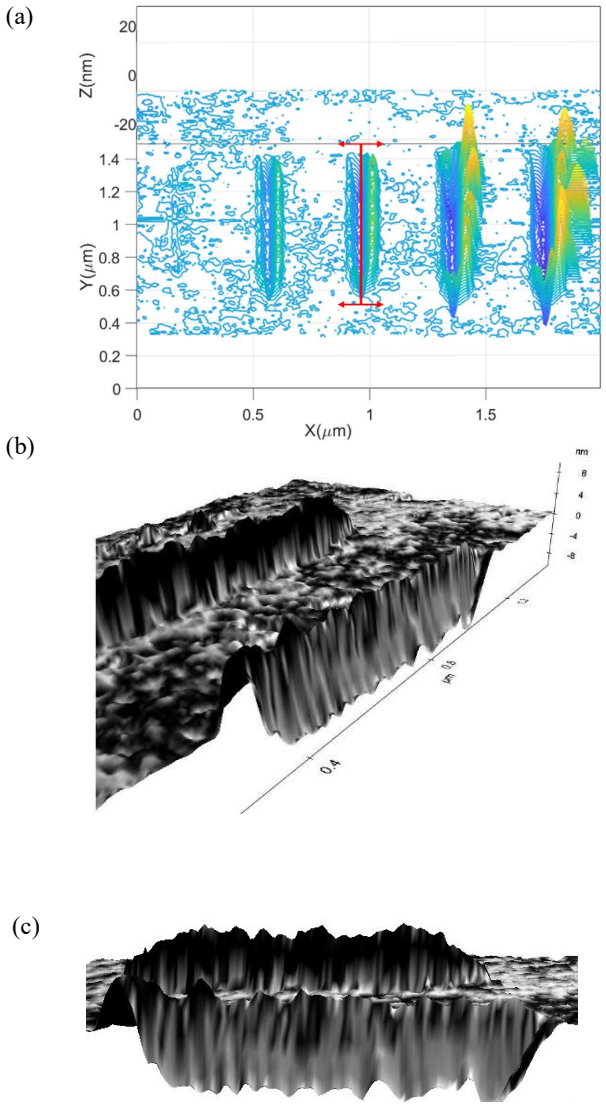

Fig. 4. (a) Top view of sample in contour line style; (b) Bird view of trench sidewall; (c) Side view of trench sidewall.

For the roughness of nanofabrication, the line edge roughness (LER) is a significant measurement for cutting-edge quality evaluation. To evaluate the sidewall roughness performance, we acquire the line edge profile at each height level (longitudinal direction) on the trenches' sidewall for the roughness analysis. In our experiments, we take 0.5 nm as height intervals for each trench, shown in Fig. 5 (a) and (b). The line edge profiles at different height levels (contour lines) of single trenches is plotted in Fig. 5 (c).

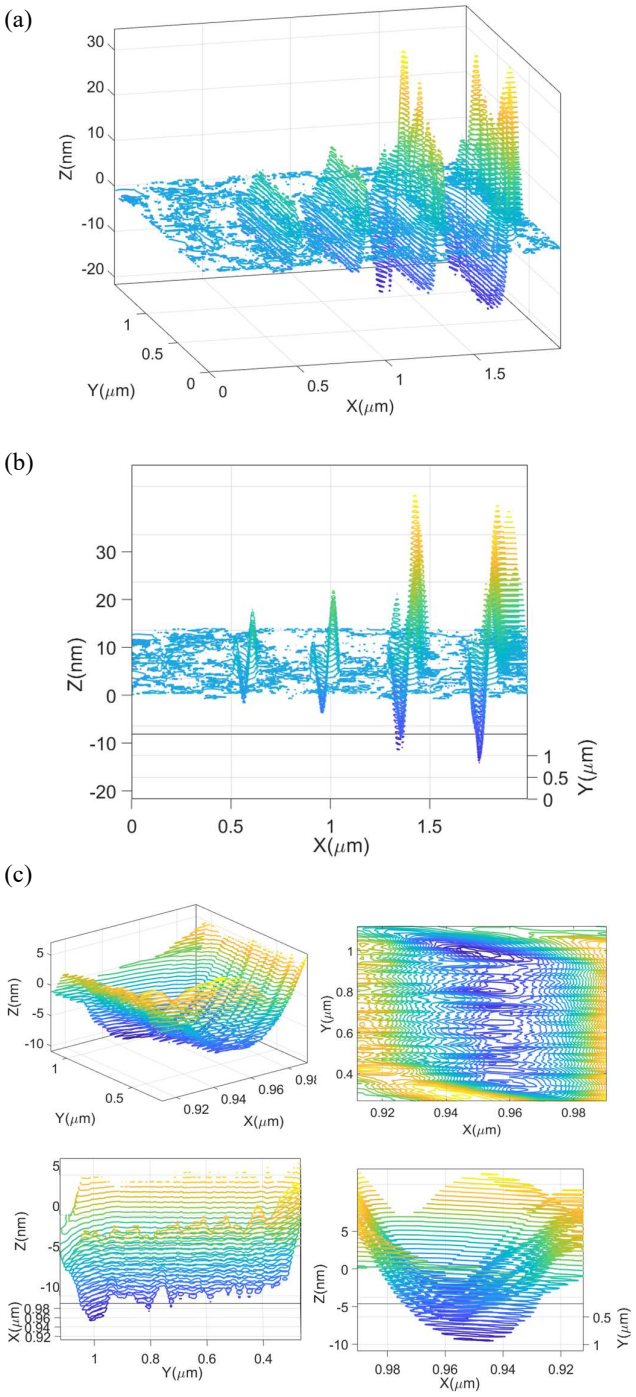

Fig. 5. (a) Bird view of sample in line edge profiles format; (b) Bird view of sample in line edge profiles format; (c) Trench in line edge profiles format.

The contour lines on the sidewall at different positions along the z-axis represent the profiles of the trenches. Analyzing the roughness changes among these line edges can indicate the sidewall quality (roughness) variation. In this experiment, we project the line edge of the sidewall on the xy-plane from the 0 z-axis position to the trench bottom with a 0.5 nm interval. To locate the position of the line edge on each trench sidewall, we assigned the index number for each line edge on the sidewall, shown in Fig. 6.

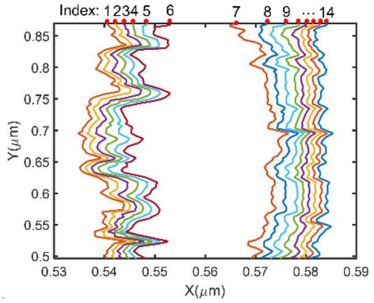

Fig. 6. The index of the line edge of the trench sidewall.

Based on the cutting results, the first trenches have poor morphology, as shown in Fig. 3, which has subtle changes in cutting depth, and the AFM cannot characterize the sidewall roughness under the nanoscale with high resolution. Therefore, it was not considered for further analysis. In addition, the cutting initiation (plunging-in) and cutting tool extraction (plunging-out) processes during the AFM nanofabrication may have inconsistency in the achieved surface characteristics; this may be due to comparable sizes of the tip rake angle, depth of cut, surface profile, and the material structure, and the resulting tool-tip geometry may possess uncertainties for the achieved cutting morphology. Therefore, the analysis does not consider the initial and ending parts of the trenches shown in Fig. 3. That is, we only adopt the middle portion of each machined nanotrench for further analysis and evaluations, and each trench's corresponding sidewall edge profiles are projected onto the xy-plane and shown in Fig. 7.

Due to the cutting depth among the trenches, the number of line edges extracted from various sidewalls differs. Each line edge's position (height level) on the trench sidewall is recorded, and the abnormal part of the trench sidewall can be marked based on the LER analysis for each line edge.

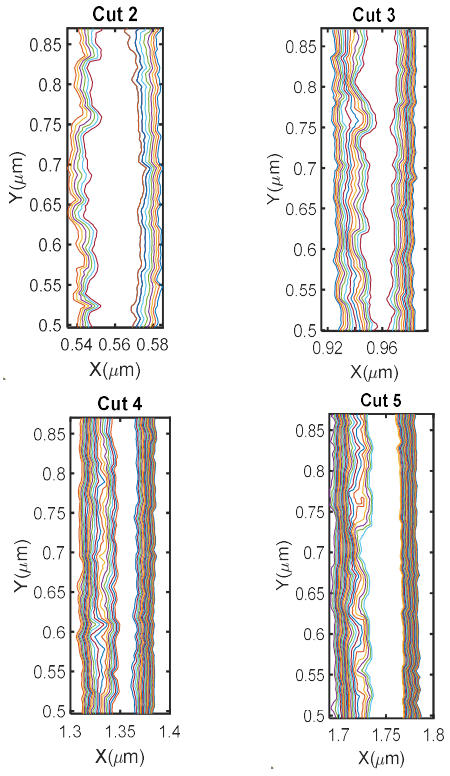

Fig. 7. Sidewall edge profiles of each trench (From Cut 2 to Cut 5).

3. Methodology

3.1. Sidewall roughness analysis using the self-affine fractal model with three parameters

LER can be regarded as variances of the sample points on the obtained line edge, which can only reflect the amplitude of the edge for roughness analysis. To accurately depict the line edge roughness, the self-affine fractal model with three parameters: the standard deviation (σ), the correlation length (ξ), and the roughness exponent (α) are used to characterize the surface roughness. Generally, the self-affine fractal model can be represented by the autocorrelation function of the line edge $R(r)$ as [30]:

$$R(r) = \sigma^2 e^{-\left(\frac{r}{\xi}\right)^{2\alpha}} \quad (1)$$

where r represents a lag distance between the two points on the edge, σ is the standard deviation of the edge profiles, the α is the roughness exponent, which can reflect the percentage changes of the high frequency feature and low frequency feature on line edge; ξ is the correlation length, which indicates the spatial feature of the edge. These three parameters are independent, and can be used to characterize a unique line edge. Therefore, these three parameters are used to detect the changes among the contour lines on the trench's sidewalls, which can indicate surface fluctuations [26].

σ can be calculated based on the coordinates of sample points on the line edge, and the ξ and α can be fitted based on the autocorrelation function (ACF), power spectral density (PSD), and height-height correlation function (HHCF) of the line edge roughness profiles [35].

The roughness profiles of the contour line on the sidewall can be treated as a data sequence as x_n $(n = 1,2,\dots,N)$ on the different positions. d is the distance between the two neighboring points. The autocorrelation function of roughness profiles $R(r)$ can be represented as:

$$R(r = md) = \frac{\frac{1}{N-m}\sum_{n=1}^{N-m}(x_{n+m} - \overline{x_n})(x_n - \overline{x_n})}{\sum_{n=1}^{N-m}(x_n - \overline{x_n})^2} \quad (2)$$

where $\overline{x_n}$ is the mean value of x_n, $m = 1,2,\dots,N-1$. ACF serves as a quantitative metric to access the randomness or periodicity of the line edge. It quantifies the correlation between the data points on the edge, and facilitates the parameter evaluation. In general, the correlation length ξ of a line edge is defined as the lag length at which the value of the autocorrelation function for this line drops to $1/e$ [36]:

$$R(\xi) = \frac{1}{e} \quad (3)$$

The correlation length ξ defines the property of the line edge roughness from the spatial perspective. If the distance between two points of the line edge is within ξ, the value of these two points can be considered correlated. Meanwhile, the relationship between the HHCF ($G(r)$) and ACF ($R(r)$) can be represented as [37]:

$$G^2(r) = 2\sigma^2[1 - R(r)] \quad (4)$$

Height-height correlation function (HHCF) is another way to express the spatial distribution of the line edge roughness profiles, which also can estimate the correlation length on the line edge and reflect the relationship between the lag distance and roughness exponent. The HHCF can be represented as [9]:

$$G(r = md) = \left[\frac{1}{N-m}\sum_{n=1}^{N-m}(x_{n+m} - x_n)^2\right]^{\frac{1}{2}} \quad (5)$$

The HHCF of each line edge is plotted, and the corresponding ξ of each line at different levels can be fitted based on the above function, shown in Fig. 8.

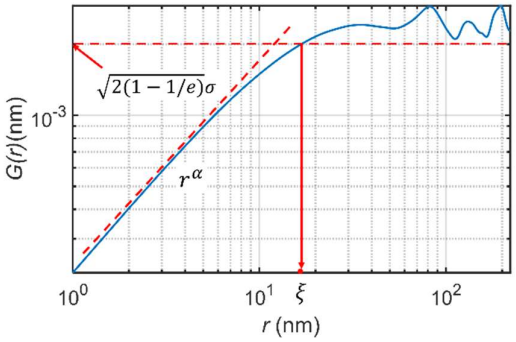

Fig. 8. HHCF of the line edge on the sidewall.

PSD analysis has become a popular method for line edge roughness, indicating the line edges high-frequency and low-frequency components. In PSD calculation, we used the discrete Fourier transform, $F(k)$, which can be represented as [38]:

$$F(k_j) = \frac{1}{N}\sum_{n=0}^{N-1} x_n e^{-\frac{2\pi i n}{N}} \quad (6)$$

where $k_j = j/N$ represents the frequency components. Due to the symmetrical property of the line edge in the frequency domain, the PSD ($P(k_j)$) can be represented as:

$$P(k_j) = 2d\left|F(k_j)\right|^2 \quad (7)$$

where $j = 1,2,\dots,N/2$, the factor of 2 is multiplied to keep the total power. The corresponding figure of the line edge roughness based on the PSD analysis is plotted in Fig. 9. The roughness exponent α can be extracted from the slope of the line, which is fitted on the short-range regime [39], where

$$S = -2\alpha - 1 \quad (8)$$

$$\alpha = \frac{-S-1}{2} \quad (9)$$

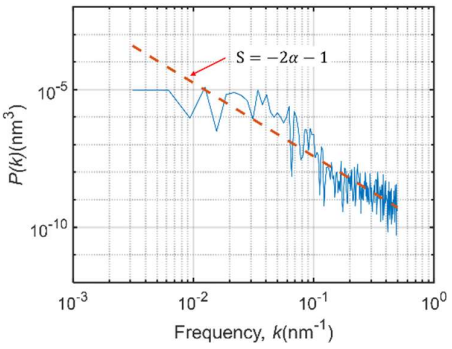

Fig. 9. PSD of the line edge on the sidewall.

Therefore, the roughness exponent α of each line edge can be fitted based on their PSD plot. After we obtained these three parameters from the corresponding functions and figures, we one can observe that the parameters of the contour lines at different locations of the trench sidewall are different, plotted based on their index in Fig. 10 (Cut 3 is taken as the example).

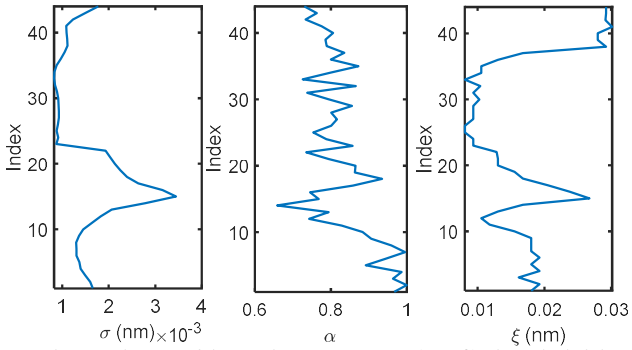

Fig. 10. Changes of the roughness parameters (σ, α, ξ) along the height index (Cut 3).

The fluctuation of the three parameters on the coordinates along the various heights of the trench sidewall reveals that the sidewall surface is not a smooth area. The changes in the parameters on coordinates can be observed, but the variation tendency of each parameter on the trench can not be summarized. To elaborate on the roughness changes on the sidewall, the statistical distribution of these three parameters will be discussed to identify the abnormal area on the sidewall, and the quality control analysis will also be applied to the sidewall of each trench.

3.2. Quality control analysis of sidewall based on the statistical distribution of parameters

The σ is the standard deviation of each line edge on the four trenches sidewall. Based on the statistical distribution analysis, the conjugate prior distribution of variance (σ^2) follows the inverse gamma distribution [40]:

$$\sigma^2 \sim Inverse - Gamma(\alpha_{IGsp}, \beta_{IGsp}) \quad (10)$$

where the α_{IGsp} is the shape parameter, and the β_{IGsp} is the scale parameter. The specific value of the α_{IGsp} and β_{IGsp} can be regarded as two non-informative prior parameters equal to 1. In addition, these two parameters also can be fitted from the existing data.

The roughness exponent α of each contour line can be calculated based on the slope S which is fitted from the PSD figures in Fig. 9. The relationship between the roughness exponent α and slope S is the linear relationship. Therefore, the statistical distribution of the α can be represented by the slope S which can be interpreted as the slope distribution in the Bayesian simple linear regression model.

Based on the previous research, the slope S statistical distribution can be defined as the student t distribution, which can be expressed as [41]:

$$S \sim t(n-2, \hat{S}, se_S) \quad (11)$$

where S represents the slope, $\hat{S}$ is the data center, and the se_S is the standard error of the S.

Based on the relationship between the slope S and α, the distribution of the α can be written as:

$$\alpha = \frac{-S-1}{2} \sim t(n-2, \frac{-\hat{S}-1}{2}, \frac{se_S}{2}) \quad (12)$$

where the distribution of the α can be defined as $\alpha \sim t(134, 0.7829, 0.0826)$.

For the ξ, we can fit the distribution curve for the obtained data ξ of contour lines. The Gamma distribution (γ) can perfectly depict the current data, which indicates that we can use the Gamma distribution to represent the statistical distribution of ξ:

$$\xi \sim \gamma(\tau, \theta) \quad (13)$$

where τ is the shape parameter, and θ is the rate parameter. The specific parameters also can be calculated from the fitted distribution line, which can be represented as $\xi \sim \gamma(3.7697, 0.0068)$.

The distribution of the three parameters is derived based on the above process, which can be used to analyze the abnormal line edge on the sidewall and achieve quality control for the sidewall roughness.

4. Results and Discussion

Based on the statistical distribution of three parameters, we can plot the quality control charts for the line edges of the trench based on each parameter. Due to the various distributions of the parameters, the outliers or the detected abnormal line edges vary among the different control charts. To incorporate these three parameters for the quality control of the sidewall, we applied the family-wise error rate (FWER) to reassign the alpha values to multiple control charts [42]:

$$FWER = Pr(rejecting\ at\ least\ one\ |H_j \in H_o) = \alpha, where\ H_o = \{H_1, H_2, .., H_k\}$$
$$\alpha_i = 1 - (1-\alpha)^{1/k} \quad (14)$$

where α_i is the new significant value to calculate the boundary of the quality control chart. The control charts are shown in Fig. 11, separated into two partitions by the green line. The left part represents the control chart acquired by the training data set (Cut 2, Cut 3, and Cut 4), which has a more consistent surface profile generated. The right part is the performance results of the testing set (Cut 5). The blue lines represent the corresponding parameter of each line edge; the red lines are the up and low boundary; the red circles mark the outliers of the data set, which can be regarded as the abnormal line edges on the sidewall.

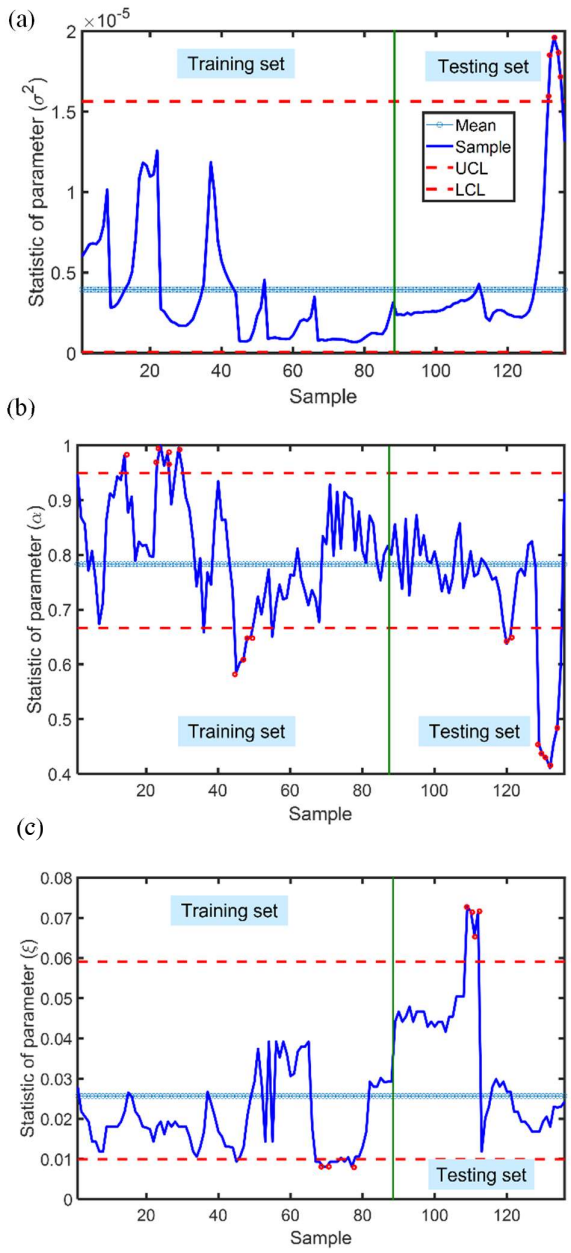

Fig. 11. (a) Quality control chart based on variance; (b) Quality control chart based on roughness exponent; (c) Quality control chart based on correlation length.

Based on the quality control chart analysis, the abnormal line edge on the trench sidewall can be detected based on the index of the outliers points on the figures and remapped to the trench sidewall. Based on the results of Fig. 11, the abnormal part can be located on the sidewall of different Cuts. In Fig. 12 (a), the trench is cut from the middle position to show the abnormal part on the left sidewall of the nanochannel (Cut 5), which is marked by red color. In Fig. 12 (b), the abnormal line edges on the sidewall acquired from the quality control chart in Fig.12 are marked in red. (Cut 5 is taken as an example to show the abnormal part of the sidewall based on the outliers in the Figures). In addition, we can also observe some abnormal line edges on Cut 4, which is marked in Fig. 12 (c). However, if the variations of the conventional surface roughness quantifier R_a does not show significant differences between the normal and abnormal sidewall morphologies (e.g., R_a=1.4151 nm for the right-hand side sidewall of Cut 5, and R_a= 1.9649 nm for its left-hand side).

Based on the statistical analysis of the parameters and quality control process for the line edge on the sidewall, the outliers indicate the abnormal regions on the achieved nanochannel, which can assist people in evaluating the quality and assessing the process performance. More importantly, the developed quality control approach allows us to identify the anomaly regions (with surface integrity issues) that need to be remanufactured, which offers the opportunity to enable the characterizations-inspection-repair/rework via the presented AFM-based nanofabrication platforms.

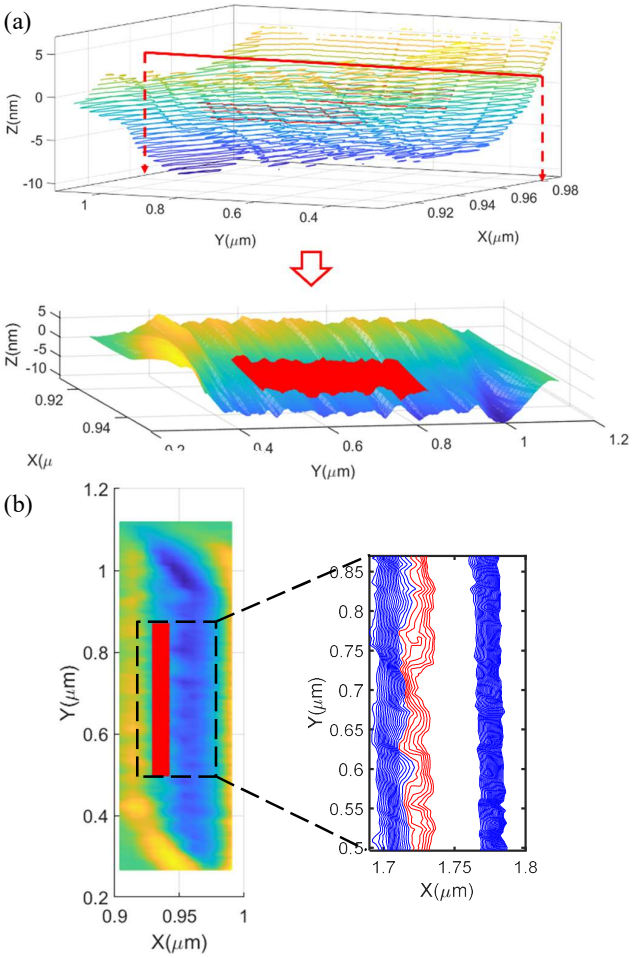

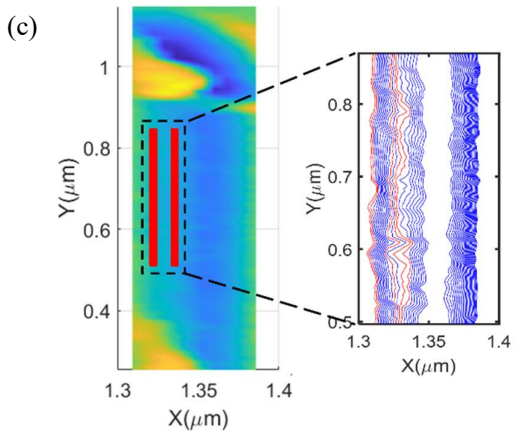

Fig. 12. (a) The abnormal area on the left sidewall of the Cut 5 trench; (b) The abnormal line edges on the left sidewall of Cut 5; (c) The abnormal line edges on the left sidewall of Cut 4.

5. Conclusions

This paper presents a quality inspection approach to evaluate the nanotrench sidewall characteristics via a statistical process control framework on the self-affine fractal model. The main contributions of this paper can be summarized as follows.

1. The roughness properties of nanochannel sidewalls can be analyzed via the self-affine fractal modeling on the line edges to reflect the roughness characteristics. In addition, the changes in these parameters along the sidewall morphology variations can indicate that the sidewall of the trench is not a smooth surface.

2. To accurately diagnose the anomaly regions on the achieved sidewalls, the quantifier, standard deviation, from the self-affine fractal model can depict the amplitude changes of the sidewall surface; the correlation length parameter is used to reflect the spatial correlations of the line edge, which can indicate the trends and frequency in the surface variations; the roughness exponent suggests contributions of high-frequency and low-frequency fluctuations on the surface characteristics.

3. The developed statistical process control based on the distributions of these three parameters can precisely locate and signify the surface profile anomalies, i.e., the rework regions on the nanochannel sidewalls.

The proposed quality control and evaluation method can effectively analyze the roughness attributes of nanochannels' sidewalls and identify anomalies on the sidewall surfaces. It offers the chance to enable quality control for AFM-based nanofabrication. In addition, it creates a route for characterization-diagnosis-rework/repair for AFM-based nanofabrication technology, which enables the cost- and time-efficiencies on the presented AFM-based nanofabrication platform.

In the future, the mechanisms of the nanofabrication will be studied based on the performance of the trenches' sidewall, including the impacts on the surface morphology inconsistency during cutting initiation and tool extraction, and the correlation between the sidewall roughness and machining parameters will be investigated to optimize the process to improve the achieved nanostructure. Meanwhile, the sidewall quality control approach can combine with the sensor-based monitoring scheme to achieve the online monitoring of the nanofabrication (based on more experimental investigations), which can effectively improve manufacturing effectiveness at the nanoscale level and reduce the damage to the sample from the testing process [32] [33].

Acknowledgment

This work was supported by the National Science Foundation No. CMMI-2006127; the Binghamton University Data Science Transdisciplinary Areas of Excellence (TAE) seed grant; the Small Scale Systems Integration and Packaging (S3IP) Center of Excellence from the New York Empire State Development's Division of Science, Technology, and Innovation.

References

[1] Yan Y, Geng Y, Hu Z. Recent advances in AFM tip-based nanomechanical machining. Int J Mach Tools Manuf 2015;99:1–18. https://doi.org/10.1016/j.ijmachtools.2015.09.004.

[2] Zhou H, Jiang Y, Ke C, Deng J. Electric-Field and Mechanical Vibration-Assisted Atomic Force Microscope-Based Nanopatterning. J Micro Nano-Manuf 2023;10. https://doi.org/10.1115/1.4056731.

[3] Zhou H, Jiang Y, Dmuchowski CM, Ke C, Deng J. Electric-Field-Assisted Contact Mode Atomic Force Microscope-Based Nanolithography With Low Stiffness Conductive Probes. J Micro Nano-Manuf 2022;10. https://doi.org/10.1115/1.4054316.

[4] Deng J, Zhang L, Dong J, Cohen PH. AFM-based 3D nanofabrication using ultrasonic vibration assisted nanomachining. J Manuf Process 2016;24:195–202. https://doi.org/10.1016/j.jmapro.2016.09.003.

[5] Fan Z, Hu X, Gao RX. Indirect Measurement Methods for Quality and Process Control in Nanomanufacturing. Nanomanufacturing Metrol 2022;5:209–29. https://doi.org/10.1007/s41871-022-00148-4.

[6] Deng J, Jiang L, Si B, Zhou H, Dong J, Cohen P. AFM-Based nanofabrication and quality inspection of three-dimensional nanotemplates for soft lithography. J Manuf Process 2021;66:565–73. https://doi.org/10.1016/j.jmapro.2021.04.051.

[7] Wang X, Liu Z, Yang Y, Cai Y, Song Q, Wang B. Effects of sidewall roughness on mixing performance of zigzag microchannels. Chem Eng Process - Process Intensif 2022;179:109057. https://doi.org/10.1016/j.cep.2022.109057.

[8] Deng J, Dong J, Cohen PH. Development and Characterization of Ultrasonic Vibration Assisted Nanomachining Process for Three-Dimensional Nanofabrication. IEEE Trans Nanotechnol 2018;17:559–66. https://doi.org/10.1109/TNANO.2018.2826841.

[9] Kizu R, Misumi I, Hirai A, Gonda S. Enhancing the precision of 3D sidewall measurements of photoresist using atomic force microscopy with a tip-tilting technique. J Appl Phys 2023;133:065302. https://doi.org/10.1063/5.0130459.

[10] Kim S-K. Line-Edge Roughness on Fin-Field-Effect-Transistor Performance for 7-nm and 5-nm Patterns. J

Nanosci Nanotechnol 2020;20:6912–5. https://doi.org/10.1166/jnn.2020.18814.
[11] Xiaobo Jiang, Runsheng Wang, Tao Yu, Jiang Chen, Ru Huang. Investigations on Line-Edge Roughness (LER) and Line-Width Roughness (LWR) in Nanoscale CMOS Technology: Part I–Modeling and Simulation Method. IEEE Trans Electron Devices 2013;60:3669–75. https://doi.org/10.1109/TED.2013.2283518.
[12] Wang R, Jiang X, Yu T, Fan J, Chen J, Pan DZ, et al. Investigations on Line-Edge Roughness (LER) and Line-Width Roughness (LWR) in Nanoscale CMOS Technology: Part II–Experimental Results and Impacts on Device Variability. IEEE Trans Electron Devices 2013;60:3676–82. https://doi.org/10.1109/TED.2013.2283517.
[13] Hamzah NA, Razak NAA, Karim MSA, Salleh SZ. Validation of a roughness parameters for defining surface roughness of prosthetic polyethylene Pe-Lite liner. Sci Rep 2022;12:2636. https://doi.org/10.1038/s41598-022-05173-3.
[14] Rao PK, Kong Z, Duty CE, Smith RJ, Kunc V, Love LJ. Assessment of Dimensional Integrity and Spatial Defect Localization in Additive Manufacturing Using Spectral Graph Theory. J Manuf Sci Eng 2015;138. https://doi.org/10.1115/1.4031574.
[15] Levi S, Schwarzband I, Kris R, Adan O, Shi E, Zhang Y, et al. Edge roughness characterization of advanced patterning processes using power spectral density analysis (PSD). In: Lin Q, Engelmann SU, editors., San Jose, California, United States: 2016, p. 97820I. https://doi.org/10.1117/12.2220814.
[16] Pu L, Wang T, Huisman TJ, Maas R, Goosen M, Dillen H, et al. Analyze line roughness sources using power spectral density (PSD). In: Adan O, Ukraintsev VA, editors. Metrol. Insp. Process Control Microlithogr. XXXIII, San Jose, United States: SPIE; 2019, p. 104. https://doi.org/10.1117/12.2516570.
[17] Mack CA. Analytic form for the power spectral density in one, two, and three dimensions. J MicroNanolithography MEMS MOEMS 2011;10:040501. https://doi.org/10.1117/1.3663567.
[18] Pérez-Ràfols F, Almqvist A. Generating randomly rough surfaces with given height probability distribution and power spectrum. Tribol Int 2019;131:591–604. https://doi.org/10.1016/j.triboint.2018.11.020.
[19] Giannatou E, Constantoudis V, Papavieros G, Papagrorgiou H, Lorusso GF, Rutigliani V, et al. Deep learning nanometrology of line edge roughness. In: Adan O, Ukraintsev VA, editors. Metrol. Insp. Process Control Microlithogr. XXXIII, San Jose, United States: SPIE; 2019, p. 109. https://doi.org/10.1117/12.2520941.
[20] Chaudhary N, Savari SA, Yeddulapalli SS. Line roughness estimation and Poisson denoising in scanning electron microscope images using deep learning. J MicroNanolithography MEMS MOEMS 2019;18:1. https://doi.org/10.1117/1.JMM.18.2.024001.
[21] Dusséaux R, Vannier E. Soil surface roughness modelling with the bidirectional autocorrelation function. Biosyst Eng 2022;220:87–102. https://doi.org/10.1016/j.biosystemseng.2022.05.012.
[22] Yamaguchi A, Komuro O. Characterization of Line Edge Roughness in Resist Patterns by Using Fourier Analysis and Auto-Correlation Function. Jpn J Appl Phys 2003;42:3763–70. https://doi.org/10.1143/JJAP.42.3763.
[23] Papalia JM, Koty D, Marchack N, Lefevre S, Yang Q, Mosden A, et al. Control of sidewall roughness formation in through-silicon via etch at non-cryogenic temperatures. Adv. Etch Technol. Process Integr. Nanopatterning XI, vol. 12056, SPIE; 2022, p. 9–17. https://doi.org/10.1117/12.2614264.
[24] Frye CD, Reinhardt CE, Donald SB, Voss LF, Harrison SE. ICP etching of GaN microstructures in a Cl2–Ar plasma with subnanometer-scale sidewall surface roughness. Mater Sci Semicond Process 2022;144:106564. https://doi.org/10.1016/j.mssp.2022.106564.
[25] Kizu R, Misumi I, Hirai A, Kinoshita K, Gonda S. Development of a metrological atomic force microscope with a tip-tilting mechanism for 3D nanometrology. Meas Sci Technol 2018;29:075005. https://doi.org/10.1088/1361-6501/aabe1a.
[26] Kizu R, Misumi I, Hirai A, Gonda S. Accurate vertical sidewall measurement by a metrological tilting-AFM for reference metrology of line edge roughness. Metrol. Insp. Process Control Microlithogr. XXXIII, vol. 10959, SPIE; 2019, p. 451–8. https://doi.org/10.1117/12.2511712.
[27] Yoo S-B, Yun S-H, Jo A-J, Cho S-J, Cho H, Lee J-H, et al. Automated measurement and analysis of sidewall roughness using three-dimensional atomic force microscopy. Appl Microsc 2022;52:1. https://doi.org/10.1186/s42649-022-00070-5.
[28] Roberts S, Ji X, Cardenas J, Corato-Zanarella M, Lipson M. Measurements and Modeling of Atomic-Scale Sidewall Roughness and Losses in Integrated Photonic Devices. Adv Opt Mater 2022;10:2102073. https://doi.org/10.1002/adom.202102073.
[29] Ju Y, Dong J, Gao F, Wang J. Evaluation of water permeability of rough fractures based on a self-affine fractal model and optimized segmentation algorithm. Adv Water Resour 2019;129:99–111. https://doi.org/10.1016/j.advwatres.2019.05.007.
[30] Kizu R, Misumi I, Hirai A, Gonda S, Takahashi S. Developmental framework of line edge roughness reference standards for next-generation functional micro-/nanostructures. Precis Eng 2023;83:152–8. https://doi.org/10.1016/j.precisioneng.2023.06.003.
[31] Mack CA. Systematic errors in the measurement of power spectral density. J MicroNanolithography MEMS MOEMS 2013;12:033016. https://doi.org/10.1117/1.JMM.12.3.033016.
[32] Wang Z, Wang X, Zhou H, Deng J. A sensor-based analytic approach for predictions of nanomachined surface profile variations via capturing temporal-spectral Acoustic Emission (AE) features for vibration-assisted Atomic Force Microscopic (AFM) based nanopatterning. Surf. Eng. Forensics, vol. 12490, SPIE; 2023, p. 30–5.
[33] Wang X, Zhou H, Deng J, Wang Z. A sensor-based monitoring approach to predict surface profile of vibration-assisted atomic force microscopy (AFM)-based nanofabrication. Manuf Lett 2023;35:1119–26. https://doi.org/10.1016/j.mfglet.2023.08.109.
[34] Ma Q, Zhou H, Deng J, Wang Z. Characterizing vibration-assisted atomic force microscopy (AFM)-based nanomachining via perception of acoustic emission

phenomena using a sensor-based real-time monitoring approach. Manuf Lett 2022;34:6–11. https://doi.org/10.1016/j.mfglet.2022.08.009.

[35] Kizu R, Misumi I, Hirai A, Gonda S. Direct comparison of line edge roughness measurements by SEM and a metrological tilting-atomic force microscopy for reference metrology. J MicroNanolithography MEMS MOEMS 2020;19:044001. https://doi.org/10.1117/1.JMM.19.4.044001.

[36] Constantoudis V, Patsis GP, Tserepi A, Gogolides E. Quantification of line-edge roughness of photoresists. II. Scaling and fractal analysis and the best roughness descriptors. J Vac Sci Technol B Microelectron Nanometer Struct Process Meas Phenom 2003;21:1019–26. https://doi.org/10.1116/1.1570844.

[37] Kizu R, Misumi I, Hirai A, Gonda S, Takahashi S. Effect of white noise on roughness measurements of self-affine fractals. Meas Sci Technol 2023;34:105003. https://doi.org/10.1088/1361-6501/ace19d.

[38] Kizu R, Misumi I, Hirai A, Gonda S. Line edge roughness measurement on vertical sidewall for reference metrology using a metrological tilting atomic force microscope. J MicroNanolithography MEMS MOEMS 2020;19:014003. https://doi.org/10.1117/1.JMM.19.1.014003.

[39] Constantoudis V, Patsis GP, Tserepi A, Gogolides E. Quantification of line-edge roughness of photoresists. II. Scaling and fractal analysis and the best roughness descriptors. J Vac Sci Technol B Microelectron Nanometer Struct Process Meas Phenom 2003;21:1019–26. https://doi.org/10.1116/1.1570844.

[40] Hayashi H, Furui A, Kurita Y, Tsuji T. A Variance Distribution Model of Surface EMG Signals Based on Inverse Gamma Distribution. IEEE Trans Biomed Eng 2017;64:2672–81. https://doi.org/10.1109/TBME.2017.2657121.

[41] Khan S, Saleh AKMdE. Estimation of Slope for Linear Regression Model with Uncertain Prior Information and Student-t Error. Commun Stat - Theory Methods 2008;37:2564–81. https://doi.org/10.1080/03610920802040399.

[42] Nicholson KJ, Sherman M, Divi SN, Bowles DR, Vaccaro AR. The Role of Family-wise Error Rate in Determining Statistical Significance. Clin Spine Surg 2022;35:222–3. https://doi.org/10.1097/BSD.0000000000001287.